Large Eddy Simulation of Wind Turbine Wakes during the Evening Transition Period

Large Eddy Simulation of Wind Turbine Wakes during the Evening Transition Period

W. Chanprasert[1], R. N. Sharma[1], J. E. Cater[2] and S. E. Norris[1]

[1]Department of Mechanical Engineering, University of Auckland, New Zealand
[2]Department of Engineering Science, University of Auckland, New Zealand

E-mail: wcha533@aucklanduni.ac.nz

Abstract.

A transient simulation of a two inline wind turbines during the evening transition period is modelled using Large Eddy Simulation with an actuator disc method. Two inline turbines are placed parallel to the stream-wise direction and the distance between the turbines is seven rotor diameters. The wind profiles and turbulence data are produced by a precursor simulation. The simulation was carried out for four physical hours and the surface heat flux varies with time according to the evening period. The wind profile evolves over the transition period and the atmospheric stability gradually changes from unstable in the late afternoon to a stable condition in the evening. The wake recovers more quickly in the afternoon and it recovers more slowly corresponding to the changes in atmospheric stability. This causes a reduction in the power output and the mean thrust load of the downstream turbine over the period. Additionally, the velocity spectrum displays higher fluctuations at the downstream turbine.

1. Introduction

Utility-scale wind turbines are typically clustered as a wind farm in order to minimise the installation, operation and maintenance costs [1]. However, the performance of downstream turbines is inevitably affected by turbulent wakes created by those upstream. The velocity deficit in the wake region reduces the power output and the high turbulence intensity increases the dynamic load on the turbine rotor.

Horizontal-Axis Wind Turbines (HAWT) operate in the atmospheric boundary layer (ABL) where the wind profiles and turbulence intensity are influenced by the surface roughness and thermal stratification of the atmosphere. Different types of stratification affect the stability of the ABL, and the boundary layer can be classified as neutral, stable or unstable, accordingly [2]. A neutral condition can be observed during strong winds when turbulence generation is dominated by shear due to the surface roughness. A stable case can occur at night when the ground loses heat by radiation and cools the air in the lowest layer of the atmosphere. This results in a stable stratification, which suppresses vertical motion and turbulence. An unstable stratification often occurs during the day when the ground is heated by the sun causing the air to rise promoting vertical motion and turbulence. The sequential development of these different stability conditions corresponds to a standard diurnal cycle.

A Large Eddy Simulation (LES) of wind turbines during a full transient diurnal cycle has been conducted in recent research [3, 4, 5]. For example, Abkar et al. [3] presented the variation of the mean power deficit of the 36-turbine wind farm where the power deficit at night was

higher than during the day. However, all of these studies focused on wake structure and power output but did not examine variations in the rotor load.

Other research has focused on wind turbine and wind farm performance only during the evening transition period ([6, 7]). This is defined by Lee and Lundquist [6] as the period when the surface heat flux changes from positive to negative sign and the ABL transforms from unstable to stable. It was also noted that electricity demand typically increases during this time; this is important for wind power prediction.

Lu et al. [7] investigated the dynamic loads on a single wind turbine during the evening transition period. The atmospheric flow was produced using LES and wind turbine loads were calculated in the aeroelastic tool FAST [8]. This work revealed the changes in the maximum and fatigue loads of a standalone turbine during the period that atmospheric stability shifts from unstable to neutral. However, since the simulation was based on a one-way coupling method, where the wind turbine was not modelled in the flow domain, the wake interactions between multiple turbines were not studied.

The present research aims to study the evolution of wind turbine wake characteristics and their effect on the variation of the power output and the rotor disc thrust loads during the evening transition period using the open-source field measurement as a transient input data. The methodology is described in section 2. This includes the governing equations, the numerical setup, the validation studies and the prescribed surface heat flux data. The simulation results of the atmospheric boundary layer and wind turbines are presented in section 3. The limitations in this study are then discussed in section 4, and this is followed by the conclusions in section 5.

2. Methodology

2.1. Large Eddy Simulation

The SnS CFD solver was used to calculate a LES of the transient turbulent ABL [9]. This code solves transient incompressible flows on structured Cartesian meshes using a Fractional step method. This simulation used the Adams-Bashforth scheme for the advective terms and Crank-Nicolson for the diffusive terms in the time stepping scheme. For spatial discretisation second order central differencing was used for both advective and diffusive terms.

LES has been widely used for wind turbine and wind farm simulations [10]. Unlike Reynolds Averaged Navier-Stokes (RANS) methods it provides details of the unsteady turbulent flow field of the wakes, while the computational cost is lower than Direct Numerical Simulation (DNS). LES resolves large eddy scales by spatially averaging the transport variables over the finite volumes of the mesh while the small eddy scales are modelled with a subgrid-scale (SGS) model. The filtered Navier-Stokes and energy equations can be written as

$$\frac{\partial \overline{u}_i}{\partial x_i} = 0, \tag{1}$$

$$\frac{\partial \overline{u}_i}{\partial t} + \overline{u}_j \frac{\partial \overline{u}_i}{\partial x_j} = -\frac{1}{\rho}\frac{\partial \overline{p}}{\partial x_i} + g\beta(\overline{\theta} - \theta_0)\delta_{i2} + \frac{\partial}{\partial x_j}\left(\nu\left(\frac{\partial \overline{u}_i}{\partial x_j} + \frac{\partial \overline{u}_j}{\partial x_i}\right) - \overline{\tau}_{ij}\right) + F_i^T. \tag{2}$$

The energy equation is formulated in terms of the potential temperature, θ,

$$\frac{\partial \overline{\theta}}{\partial t} + \overline{u}_i \frac{\partial \overline{\theta}}{\partial x_i} = \frac{\partial}{\partial x_j}\left(D\frac{\partial \overline{\theta}}{\partial x_i} - q_j\right). \tag{3}$$

The F_i^T term is the body force exerted by the turbine model. The term $\overline{\tau}_{ij}$ in Equation 2 is the subgrid-scale stress

$$\overline{\tau}_{ij} = \nu_{SGS}\left(\frac{\partial \overline{u}_i}{\partial x_j} + \frac{\partial \overline{u}_j}{\partial x_i}\right), \tag{4}$$

and the q_i in Equation 3 is the subgrid-scale heat flux. Here ν_{SGS} is the subgrid-scale viscosity:

$$\overline{q_i} = -\frac{\nu_{SGS}}{Pr_t}\frac{\partial \overline{\theta}}{\partial x_i}. \tag{5}$$

In this study, the SGS turbulence is modelled using a constant Smagorinsky model [11] with a coefficient of 0.13 following Churchfield et al. [12].

2.2. ABL and Wind Turbine Modelling

There are two steps in the simulation sequence; in the first step, the wind profile and turbulence data were produced by a precursor simulation in which the flow was calculated using a pressure-driven periodic boundary condition for an empty domain. The computational domain size was $19D \times 7D \times 8D$ in the x, y, z directions with a mesh size of $\frac{1}{8}D \times \frac{1}{12}D \times \frac{1}{20}D$ where D is the turbine rotor diameter. A schematic of the domain is shown in figure 1.

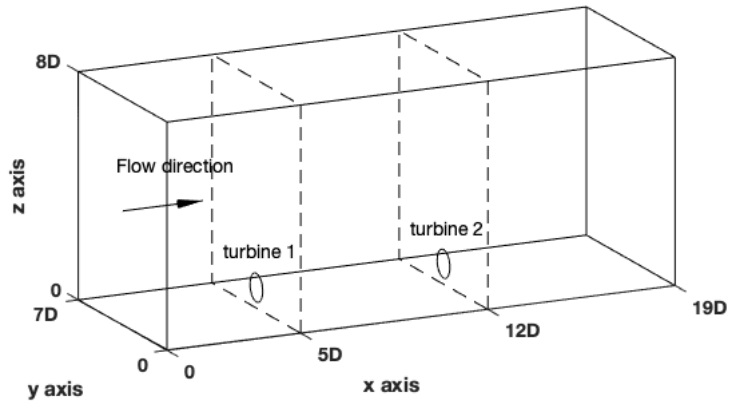

Figure 1: Computational domain of the two turbines model showing the distances non-dimensionalised by the turbine rotor diameter, D.

The bottom boundary condition was specified as a rough wall using a wall function with a surface roughness, z_0, of 0.05 m which is typical for farmland terrain [13], and the surface heat flux varied as a function of time. The top boundary was set to be stress free and adiabatic. The initial velocity and temperature fields for the transient surface heat flux precursor run were obtained from a separate quasi-steady run using a constant surface heat flux that match to the heat flux at the beginning of the transition period. For this precursor run, the velocity field was initialised with a logarithmic profile and the initial potential temperature was set at a constant value of 300 K. The precursor simulation a duration of 20,000 seconds, which was found to be long enough to obtain a quasi-steady state flow.

In the subsequent simulation, the horizontal inflow mean wind speed at hub-height was controlled to 9 m/s throughout the transient simulation [5]. This was done by adjusting the pressure gradient relative to the error between the planar-averaged actual velocity and the target velocity at hub-height at every time step. This wind speed caused the turbines to operate in the Region 2 of the power curve where the thrust coefficient between wind speed of 7.8 and 10.3 m/s is approximately constant [14]. The wind speed at hub-height was fixed to determine the effects of atmospheric stability on the wind shear profiles and turbulence. The Coriolis effect was not modelled since the turbine model used in this study is situated below the Ekman layer. The Coriolis force is not expected to have a significant impact on a single wind farm simulation [15]. Velocity data at a cross-stream plane at the inlet was recorded every 1 second which is used for the inlet boundary condition of wind turbine simulations.

In the second step, the NREL 5-MW reference turbine which has a rotor diameter, D, of 126 m and a hub-height, H, of 90 m [14] was used. Two turbines were placed inline in the stream-wise direction and the distance between two turbines was 7 rotor diameters. The turbines were modelled in the flow domain using an actuator disc model without rotation, as implemented by Norris et al. [16]. The mesh size around the discs was refined to $\frac{1}{40}D \times \frac{1}{40}D \times \frac{1}{40}D$ in order to adequately model the turbulent wakes. The total actuator disc thrust force can be calculated from:

$$F_T = C_T \frac{1}{2} \rho U_\infty^2 A_T, \tag{6}$$

where A_T is the disc surface area and U_∞ is the free-stream wind velocity. For the wind turbine simulations, the velocity at the downstream turbine is affected by the turbulent wake of the upstream and the U_∞ is not a meaningful choice. Hence, the area-averaged velocity at rotor disc, U_d, is used and the free-stream velocity is calculated from the induction factor, a, according to one-dimensional momentum theory:

$$U_\infty = \frac{U_d}{1-a}. \tag{7}$$

Equation 6 is therefore modified:

$$F_T = C_T \frac{1}{2} \frac{\rho U_d^2 A_T}{(1-a)^2}. \tag{8}$$

A constant thrust coefficient of 0.75 and an induction factor of 0.25 were used [17]. However, in this work, the tangential forces were also implemented using the NREL 5MW turbine torque curve. These were updated every time step as a function of the wind speed at the rotor hub. The forces were uniformly distributed across the disc radius and the forces were distributed to the computational mesh using an existing method [18]. The aim of this estimate was to obtain a swirl flow, it was not intended to accurately calculate the torque and power of the wind turbines. The recorded data at the cross-stream plane from the precursor simulation was used for the inlet boundary condition. The outlet boundary downwind was set to zero-pressure. A periodic boundary was used for the span-wise boundaries.

2.3. LES Validation

The SnS code has been validated a the neutrally stratified atmospheric boundary layer [16, 19], however the code has not been used for non-neutral atmospheric conditions. Therefore, a validation study was conducted using other LES simulation results for a quasi-steady simulation and using observation data for a transient ABL.

Quasi-steady Simulation: A quasi-steady simulation was carried out for neutral, unstable and stable stratifications, and compared with the precursor simulation results of Ghaisas et al. [20] who used the SOWFA code which has been verified and validated for thermally stratified ABL. In this study, the ground was modelled using a rough wall function with a surface roughness of 0.016 m. The surface heat flux was zero for the neutral case and a constant value of 0.04 K-m/s for the unstable case. For the stable case, the temperature at the bottom surface was reduced at a constant rate of -0.25 K/hr. The mean wind speed at the turbine hub-height was controlled to 9 m/s for all three simulations. The simulated durations were 12000 seconds and statistical data was calculated during the final 2000 seconds.

Figure 2 shows the mean stream-wise velocity profiles for neutral, unstable and stable conditions compared to Ghaisas et al.[20] and the Busiger-Dyer relationships. The SnS code predicts similar wind profiles to Ghaisas et al.[20] particularly at the turbine rotor height.

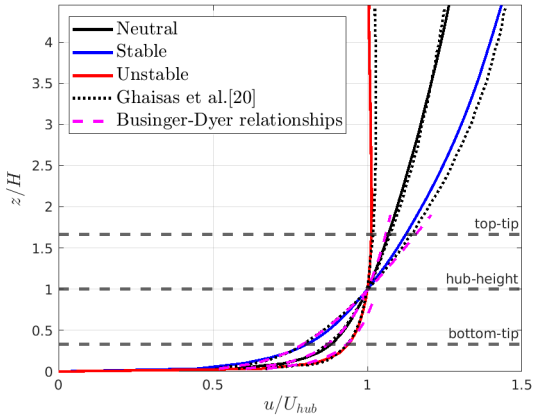

Figure 2: The mean stream-wise velocity profile in the vertical plane for the neutral (black solid line), stable (blue solid line) and unstable (red solid line) conditions, compared with Ghaisas et al. [20] (black dotted lines) and the log-law profile with different thermal stability (pink dashed lines).

Transient Simulation: The transient ABL during the evening transition period was simulated and compared with the observation data of Lee and Lundquist [6] which was recorded on 9 July 2011 at a wind farm in central Iowa. Unlike the earlier precursor simulation in section 2.2, the wind speed at hub-height was not controlled, but instead a constant pressure gradient in the stream-wise direction was applied.

Figure 3 shows the comparison between observation data and the LES results for wind speed at 80 m height, corresponding to the change of surface heat flux during the evening period. LES can capture the overall trend of the wind speed, however it over-predicts at after 19.00 by approximately 1 m/s. Figure 4 compares the 2-min mean vertical wind profiles of observation data and LES results at 17.30, 18.30 and 19.30. LES calculates a reasonable value of the wind shear during the evening.

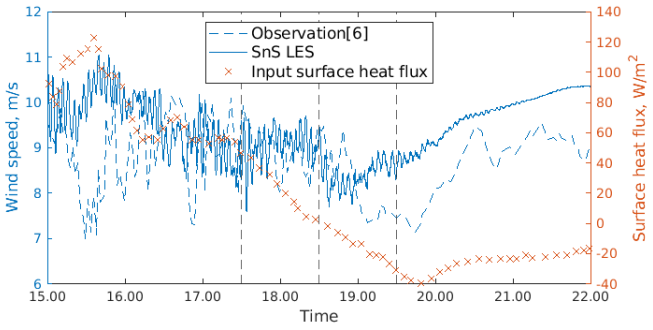

Figure 3: Comparison between observation data [6] (dashed blue line) and LES result (solid blue line) of wind speed at 80 m height. The surface sensible heat fluxes are displayed with red crosses. The three vertical dashed lines mark the time period for which the wind profiles are compared.

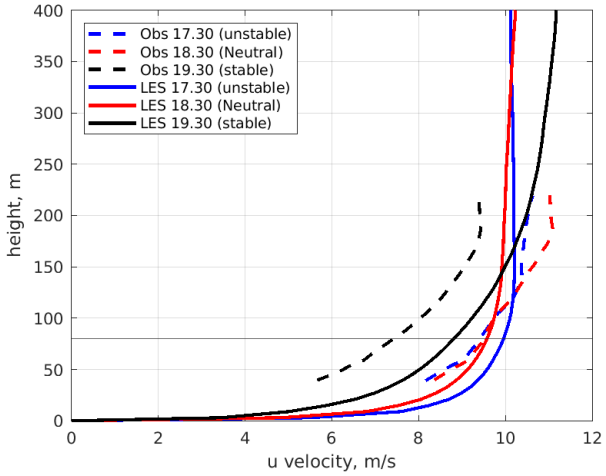

Figure 4: Comparison between observation data [6] (dashed lines) and LES results (solid lines) for stream-wise velocity profiles at 17.30, 18.30 and 19.30.

2.4. NWTC M5 Meteorological Tower

The National Wind Technology Center (NWTC) M5 tower is a research meteorological tower measuring the atmospheric conditions and the inflow wind at the NWTC wind turbine test site near Boulder, Colorado. The 135m-height tower is equipped with a range of instrumentation such as cup anemometers, sonic anemometers, resistance temperature detectors (RTD) and wind vanes [21]. The surface heat fluxes are estimated from the co-located velocity and temperature measurements from the sonic anemometers [22].

The surface heat flux data used in this study were collected during July 2019. The data was processed by taking an hourly average to obtain the mean values that are used for the transient boundary condition. These data are shown in the Figure 5.

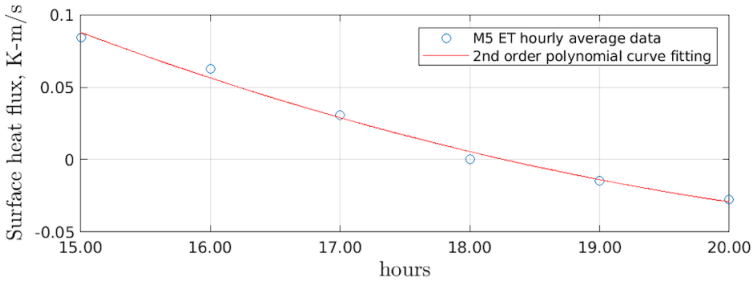

Figure 5: The variations in surface heat flux during evening period obtained from NWTC M5 tower.

3. Results

3.1. ABL Evolution during Evening Transition Period

The simulation was carried out for 4 hours of physical time from 16.00 to 20.00. The sensible surface heat flux decreases as a function of time from the positive value of 0.06 Km/s to the negative value of -0.03 Km/s. During each hour of simulated time, the flow variables were averaged over blocks of 1800 s to obtain statistical data. The results of transient ABL modelling shows the evolution of free-stream wind profiles over the evening period. The average

friction velocity, wind shear exponent, turbulence kinetic energy (TKE) at the hub-height, the Obukhov length and the stability class corresponding to each hour are tabulated in Table 1. The Obukhov length is a length scale which represents the ratio between the shear and the buoyancy in the TKE production. The value is negative for unstable stratification, positive for the stable stratification and approaches infinity for near-neutral condition. The Obukhov length is calculated from:

$$L = -\frac{\theta_0 u_*^3}{\kappa g \overline{v'\theta'}}, \tag{9}$$

where θ_0 is the reference temperature, κ is the von Karman constant which has a value of 0.41, and g is the gravitational acceleration which has a value of 9.81 m/s^2. In this study, the stability is classified by the Obukhov length [23]. The hourly averaged values as a function of time are summarized in Table 1.

Table 1: Hourly Averaged Parameters

Time	q_s $[Km/s]$	u_* $[m/s]$	α	TKE $[m^2/s^2]$	L $[m]$	Stability class
16.15 - 16.45	0.042	0.536	0.065	0.79	-272	Unstable
17.15 - 17.45	0.017	0.517	0.073	0.73	-616	Weakly unstable
18.15 - 18.45	-0.005	0.477	0.124	0.52	1732	Neutral
19.15 - 19.45	-0.022	0.370	0.216	0.11	171	Stable

Figure 6 shows the evolution of the time averaged velocity profile from late afternoon to late evening. The wind shear changes significantly particularly at the turbine rotor height. The wind shear is lower in the first simulation hour where the velocity is approximately constant across the rotor disc. As the atmospheric stability is more stable in the evening, the wind shear increases as the wind speed at the rotor disc top is significantly higher than at the bottom.

The changes in potential temperature profile are shown in Figure 7. The temperature increases from the first hour to the second hour, then as the surface heat flux changes from positive to negative, the potential temperature near the surface reduces in the third and fourth hour while the temperature in the upper region (above 3 times the hub-height) remains constant.

The turbulence level in the atmosphere reduces as the ABL becomes more stable in the late evening and this can be seen in the turbulent kinetic energy plot in the Figure 8. Similarly, Figure 9 shows the reduction in the stream-wise turbulence intensity during the evening period where the turbulence intensity at the hub height reduces from approximately 8% in the afternoon to 4% in late evening.

3.2. Wake Interactions and Turbine Performance

In the wind turbine simulation, two inline turbines were modelled to study the effects of turbulent wakes on the downstream turbine. The simulations show that the wake deficits are larger as the ABL develops a stable condition in the late evening. Figure 10 shows the velocity deficit at each hour at hub-height in the stream-wise direction from upstream of the first turbine to the second turbine rotor location. The wake recovers more rapidly during the afternoon since the ABL is more unstable and has higher turbulence level that leads to more turbulent mixing in the wake.

The TKE at the top of the disc during the most unstable condition in the afternoon and the most stable condition in the late evening are compared in Figure 11. The pattern of the TKE profiles in the stream-wise direction are different for these two hours. For the unstable case in the afternoon, the TKE increases to a peak at approximately 1D downwind of the rotor and then decays corresponding to wake recovery. For the stable condition in the evening, the TKE gradually rises after passing the disc and remain approximately constant after 4D downwind

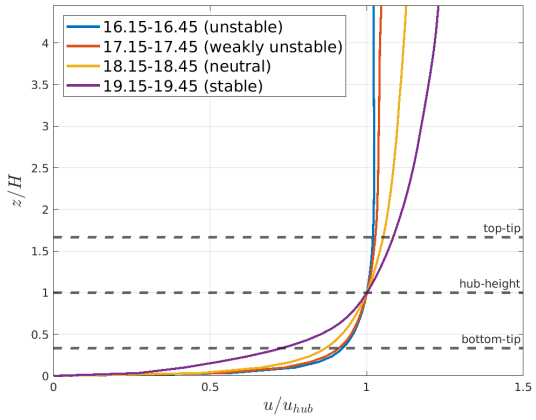

Figure 6: Mean horizontal velocity

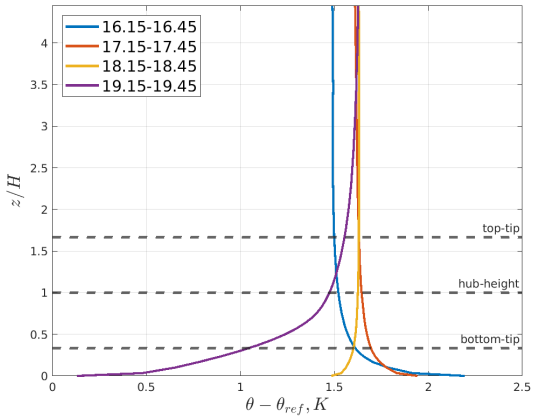

Figure 7: Mean potential temperature

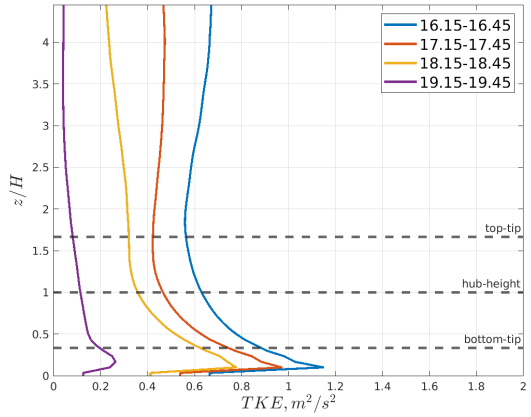

Figure 8: Turbulent kinetic energy

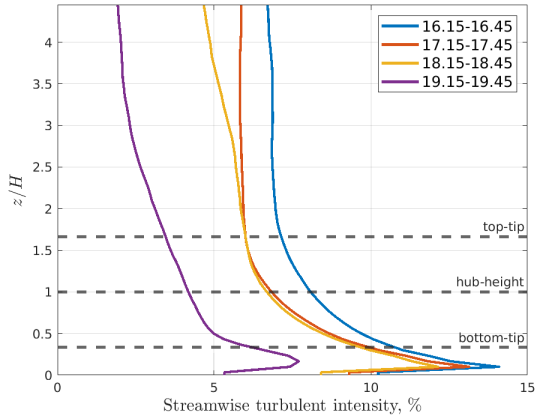

Figure 9: Stream-wise turbulence intensity

until it reaches the second turbine. However, the ambient turbulence values are different between those two hours due to the stability changes, hence the TKE at the second turbine during the first hour remains higher than the last hour.

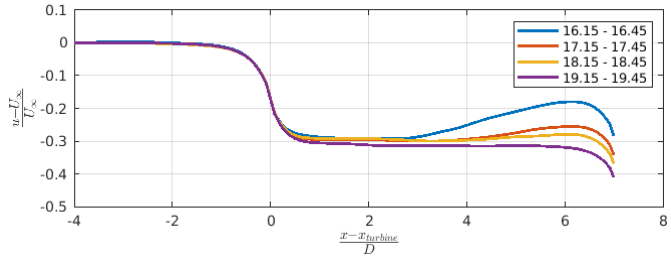

Figure 10: The velocity deficit at the hub-height in the stream-wise direction from upstream of the first turbine to the second turbine location. The first turbine is located at $\frac{x-x_{loc}}{D} = 0$ and the second turbine is at $\frac{x-x_{loc}}{D} = 7$.

In order to investigate the performance of the downstream turbine, the power output and the mean rotor disc thrust load are normalised by the upstream turbine and are called the relative

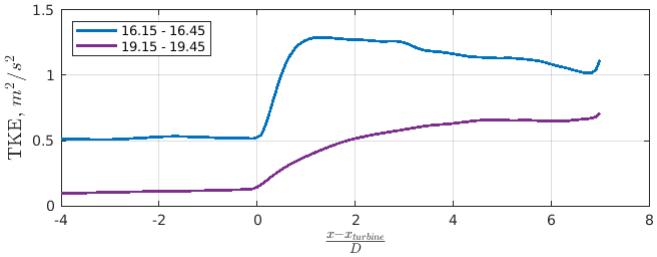

Figure 11: The turbulence kinetic energy at the top-tip height in the stream-wise direction from upstream of the first turbine to the second turbine location. The first turbine is located at $\frac{x-x_{loc}}{D} = 0$ and the second turbine is at $\frac{x-x_{loc}}{D} = 7$ position.

power output (P_{Rel}) and relative mean rotor thrust load ($F_{T,Rel}$) respectively. The relative power output decreases from approximately 70% in an unstable ABL to 30% in a stable ABL while the relative mean load drops from 80% to less than 50%. This is because the turbine wake recovers faster under unstable conditions and result in a higher wind speed at the downstream rotor disc. This demonstrates the significant change in power generation and the mean rotor load due to the wind profile across the transition period.

However, the mean thrust load does not represent a realistic load on the rotor disc because turbulent wakes consist of different sized eddies which create fatigue loads. Figure 13 shows the power spectra of stream-wise velocity fluctuations upstream of the first and second wind turbines. The Fast-Fourier Transform (FFT) was performed over a 10-min interval of the time series data which are extracted from the monitor points at rotor top height. The magnitudes of the velocity spectra of the downstream turbine are higher than the upstream turbine at all frequencies. This indicates that the downstream turbine experiences higher fluctuating forces. Nonetheless, more advanced fatigue analysis needs to be undertaken in order to estimate the Damage Equivalent Load (DEL) on the turbines.

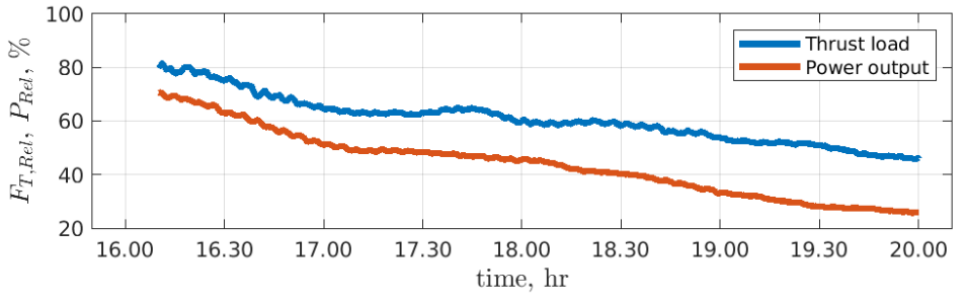

Figure 12: The variation of the power output and the rotor thrust load of the downstream turbine relative to the upstream turbine during the evening transition period.

Figure 14 illustrates the wake structure of two inline turbines during the last hour of the simulated time. The shear layer of the downstream turbine breaks down more rapidly due to the higher turbulence level in the wake created by the upstream turbine.

4. Discussion

Initially, results from a simulation of an empty domain was validated with observation data. The LES model correctly predicted the trends in the wind speed at the hub-height and the wind profiles during the course of the transition period. However, there are constraints that affect the

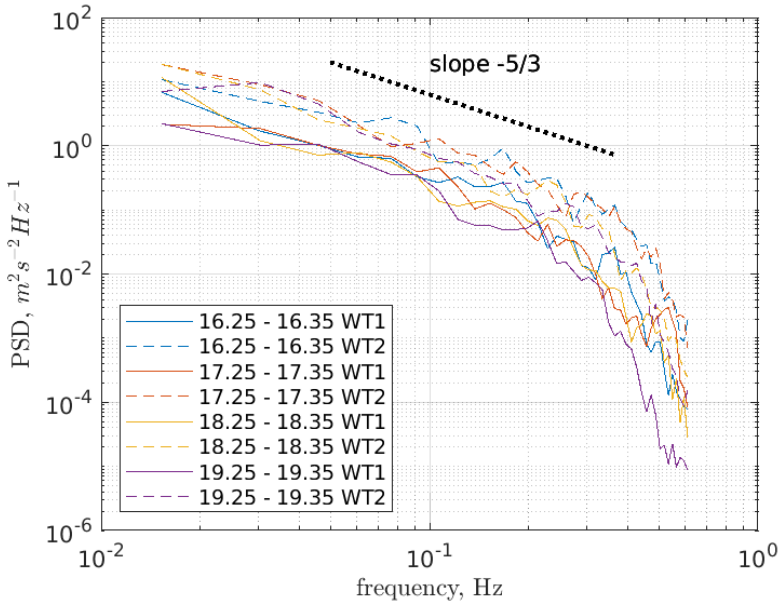

Figure 13: The power spectra of stream-wise velocity fluctuation at 0.5D upstream of the first (solid lines) and second turbine (dashed lines) for each simulated hour at rotor top height.

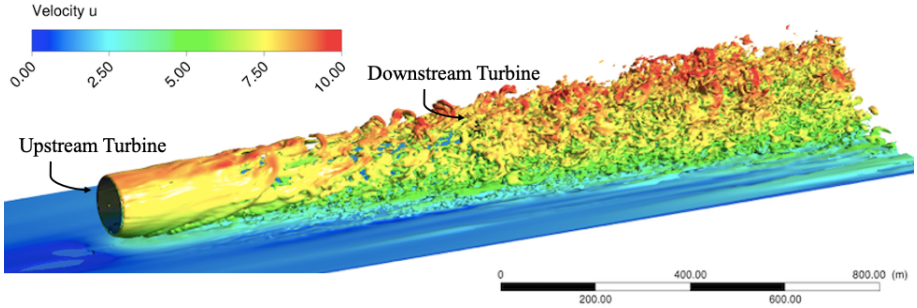

Figure 14: Instantaneous iso-surface of vorticity magnitude ($\omega = 0.2\ s^{-1}$) coloured by the stream-wise velocity during the last hour of the simulated period.

accuracy in the simulations. Firstly, the effects of geostrophic winds and mesoscale advection terms were not able to modelled since a mesoscale model was not coupled. Hence, only the surface heat flux variations could be modelled, while the changes in the geostrophic wind during the evening period were not simulated.

Secondly, the Coriolis effect was not implemented in this model since the focus was put on the wind turbine region which is located below the Ekman layer. This means that the Low-Level Jet (LLJ) which is typically observed during the night could not be modelled. The LLJ is a stream of wind near surface that has a higher speed than the geostrophic wind. It is caused by an inertial oscillation which is induced by the Coriolis force during the night as the stable ABL has less friction due to less turbulent mixing [24].

Finally, a constant Smagorinsky SGS model was used as this is a limitation of the CFD package. This standard model is less accurate than dynamic models [25], especially for the stably stratified ABL. In future work, more sophisticated SGS models and the Coriolis effect will be incorporated into the model.

5. Conclusions

Transient ABL modelling of the evening period revealed significant changes in the wind shear and the turbulence level of the free-stream flow. The changes in the atmospheric stability during the evening affects the turbine array operations by altering the wake recovery distance. The wake recovers most rapidly during the first hour of simulation and more slowly as the ABL shifts towards the stable regime. The TKE at the rotor disc top is different for the most unstable condition in the afternoon and the most stable in the late evening. The performance of the downstream turbine operated in a full wake was investigated and the results show that the power generation drops more than 40% during the evening transition period while the mean rotor thrust load reduces by approximately 30%. The velocity spectrum demonstrated a higher fluctuating dynamic load on the downstream turbine. Further study will be carried out to analyse fatigue loading of both upstream and downstream turbines in order to estimate the damage equivalent loads.

Acknowledgments

The authors would like to acknowledge the NREL's National Wind Technology Center for providing the meteorological M5 tower data which is available to download at `https://wind.nrel.gov/MetData/135mData/M5Twr/`. The authors acknowledge New Zealand's eScience Infrastructure (NeSI) for providing High Performance Computing facilities.

References

[1] Sørensen J N 2011 *Annual Review of Fluid Mechanics* **43** 427–448
[2] Burton T, Jenkins N, Sharpe D and Bossanyi E 2011 *Wind Energy Handbook (2nd Edition)* (John Wiley & Sons)
[3] Abkar M, Sharifi A and Porté-Agel F 2016 *Journal of Turbulence* **17** 420–441
[4] Englberger A and Dörnbrack A 2018 *Boundary-layer meteorology* **166** 423–448
[5] Tian L, Song Y, Zhao N, Shen W, Wang T and Zhu C 2020 *Renewable Energy* **145** 419 – 427 ISSN 0960-1481
[6] Lee J C and Lundquist J K 2017 *Boundary-Layer Meteorology* **164** 449–474
[7] Lu N Y, Basu S and Manuel L 2019 *Wind Energy* 1 – 22
[8] Jonkman J and Buhl M L 2005 FAST user's guide NREL Tech. rep. TP-500-38230, National Renewable Energy Lab.(NREL), Golden, CO (United States)
[9] Norris S 2000 *A Parallel Navier-Stokes Solver for Natural Convection and Free Surface Flow* Ph.D. thesis University of Sydney. Engineering
[10] Mehta D, Van Zuijlen A, Koren B, Holierhoek J and Bijl H 2014 *Journal of Wind Engineering and Industrial Aerodynamics* **133** 1–17
[11] Smagorinsky J 1963 *Monthly Weather Review* **91** 99–164
[12] Churchfield M J, Lee S, Michalakes J and Moriarty P J 2012 *Journal of turbulence* N14
[13] Stull R B 2012 *An introduction to boundary layer meteorology* (Springer Science & Business Media)
[14] Jonkman J, Butterfield S, Musial W and Scott G 2009 Definition of a 5-MW reference wind turbine for offshore system development Tech. rep. NREL/TP-500-38060, National Renewable Energy Lab.(NREL), Golden, CO (United States)
[15] Van der Laan M, Hansen K S, Sørensen N N and Réthoré P E 2015 *Journal of Physics: Conference Series* **625** 012026
[16] Norris S E, Cater J E, Stol K A and Unsworth C 2010 *Proceedings of the 17th Australasian Fluid Mechanics Conference*
[17] Calaf M, Meneveau C and Meyers J 2010 *Physics of Fluids* **22** 015110
[18] Rethore P E M and Sørensen N N 2008 *2008 European Wind Energy Conference and Exhibition* (European Wind Energy Association (EWEA))
[19] Storey R 2014 *Large Eddy Simulation of Dynamically Controlled Wind Turbine Arrays* Ph.D. thesis The University of Auckland
[20] Ghaisas N S, Archer C L, Xie S, Wu S and Maguire E 2017 *Wind Energy* **20** 1227–1240
[21] Clifton A 2016 135-m meteorological towers at the national wind technology center Tech. rep. NREL/TP-500-55915, National Renewable Energy Lab.(NREL), Golden, CO (United States)
[22] Hamilton N and Debnath M C 2019 National wind technology center-characterization of atmospheric

conditions Tech. rep. NREL/TP-5000-72091, National Renewable Energy Lab.(NREL), Golden, CO (United States)
[23] Wharton S and Lundquist J K 2012 *Wind Energy* **15** 525–546
[24] Van de Wiel B J, Moene A, Steeneveld G, Baas P, Bosveld F and Holtslag A 2010 *Journal of the Atmospheric Sciences* **67** 2679–2689
[25] Stoll R and Porté-Agel F 2008 *Boundary-Layer Meteorology* **126** 1–28